

# From Nuclear Structure to Nucleon Structure

Keh-Fei Liu <sup>1</sup>

*Dept. of Physics and Astronomy  
Center for Computational Sciences  
University of Kentucky, Lexington, KY 40506, USA*

---

## Abstract

Similarities between nuclear structure study with many-body theory approach and nucleon structure calculations with lattice QCD are pointed out. We will give an example of how to obtain the connected sea partons from a combination of the experimental data, a global fit of parton distribution functions and a lattice calculation. We also present a complete calculation of the quark and glue decomposition of the proton momentum and angular momentum in the quenched approximation. It is found that the quark orbital angular momentum constitutes about 50% of the proton spin.

*Keywords:* Nuclear structure, nucleon structure, quantum chromodynamics, quark and glue momentum and angular momentum

*PACS:* 21.60.jz, 24.10.Cn, 24.30. Cz, 12.38. Gc, 12.38.-t

---

## 1. In Memoriam

This manuscript is dedicated to the memory of Gerald E. Brown who was my Ph. D. thesis advisor, a mentor in my professional career and a lifelong friend.

I first met Gerry in the Fall of 1972 when I was a graduate student in Stony Brook. He just returned from NORDITA. He summoned me to his office one day and asked me if I could do some calculation for him. The problem is calculating the spectrum of two nucleons in the orbital  $j$  with a delta function interaction. The next day, I went to show him my results. He

---

<sup>1</sup>liu@pa.uky.edu

had a look and said “ The gap between the  $0^+$  and  $2^+$  states is a factor of 2 of that between  $2^+$  and  $4^+$ . OK, you can work for me now. ” I did not know it was a test to help him decide whether he wanted to take me on as his research assistant.

Gerry is well known for many insightful quotations about physics. Let me relate one which is attributed to him and it may not have been recorded in a written form before. During the opening talk at one Few Body Conference, Gerry was quoted to have said “In classical physics, you cannot solve three-body problem. With quantum mechanics, you cannot solve two-body problem and with relativistic quantum mechanics, you cannot solve one-body problem. In quantum field theory, you don’t know how to solve the vacuum.” Following Gerry’s logic, we can now append his quote by “With the advent of string theory, you no longer know where the vacuum is.”

I have learned many-body theory and Landau’s fermi-liquid theory under Gerry and my Ph. D. thesis was on a self-consistent RPA calculation of nuclear giant resonances on Hartree-Fock ground states. In the later years, I have followed Gerry to work on chiral soliton model of the nucleon, particularly the skyrmion. The many intriguing properties of the nucleon both theoretically and experimentally have led me to work on lattice quantum chromodynamics (QCD) calculation since the late eighties.

From 1995 to 2009, we have been meeting in Caltech every January as part of a contingent of theory guests, courtesy of Bob KcKeown and Brad Phillipone of the Kellogg Lab. During these visits, Gerry would explain to me his work in black holes and heavy ion collisions and I would update him on the progress in lattice QCD. Over the years, I would like to think that I have inherited part of his extraordinary enthusiasm and love for physics through osmosis and I have been influenced greatly by his way of dissecting and tackling a complex problem through intuition, backed by estimation.

It is natural to extend the study from nuclear structure to nucleon structure, especially when there is an excellent tool in lattice QCD. I am indebted to Gerry for introducing me to the fascinating world of nuclear and nucleon structures. I would like take this opportunity to thank him for his encouragement and support over the years.

## 2. Introduction

Historically, the study of nuclear structure started out from models like the liquid-drop model, the collective models and the shell model. The modern approaches include many-body theory, Green's function Monte Carlo and lattice effective theory calculation. Similarly, the study of nucleon structure progressed from quark model, MIT bag model, chiral soliton model, QCD sum rules, instanton liquid model to the more recent lattice QCD calculation. The latter is an *ab initio* Euclidean path-integral calculation of QCD with controllable statistical and systematic errors. I will make a comparison between the many-body theory approach to nuclear structure and the lattice QCD approach to nucleon structure. I will draw some parallels of the two approaches and point out some differences.

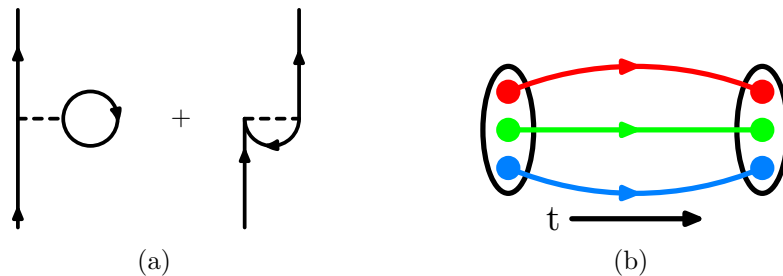


Figure 1: (a) Hartree-Fock diagrams and (b) quark skeleton diagram of quenched QCD.

Many-body theory is a non-relativistic quantum field theory, while QCD is a relativistic quantum field theory. As such, concepts like valence and sea degrees of freedom, collective phenomenon, and vacuum polarization are common, albeit in different contexts. In the case of nucleus, the first order of approximation is the mean-field description of the ground state of Fermi sea, such as the shell model or the Hartree-Fock approximation as depicted in Fig. 1a and the nucleon quasi-particle and -hole states around the Fermi sea interact via an effective interaction. This is analogous to the quenched approximation of lattice QCD where the partition function is approximated by the gauge action only without the fermion determinant as depicted in Fig. refquenched. Nucleon properties are calculated with the multi-point correlation functions with the 3-quark interpolation field for the source and sink of the nucleon at distant time slices in the pure gauge background.

More refined approaches to nuclear structure to take into account the particle-hole excitation include single particle renormalization with particle-phonon coupling [1, 2] and Kuo-Brown interaction of the valence nucleons via core excitation of phonons [3]. These are illustrated in Fig. 2a. On the nucleon structure side, the analogy would be the incorporation of the dynamical fermions in the gauge background field with quark loops in the vacuum which represent the fermion determinant in the partition function. This is drawn schematically in Fig. 2b.

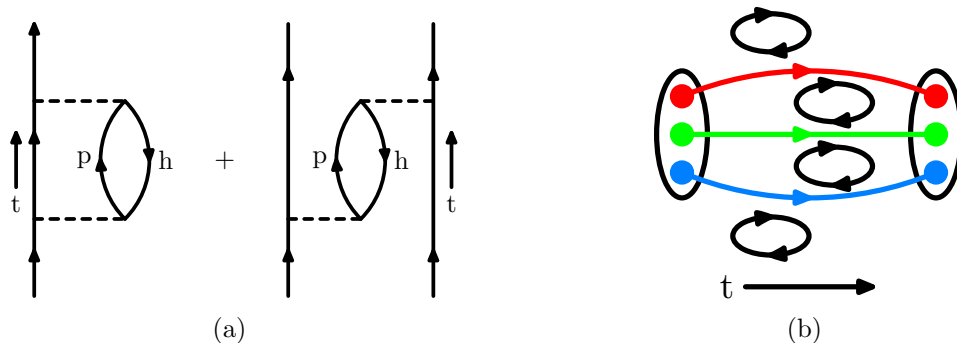


Figure 2: (a) Particle-phonon coupling and core excitation and (b) Lattice QCD with dynamical fermions.

We shall show that there are parallel developments of the same concepts in dynamics as well as classification of degrees of freedom in many-body theory and QCD, since both are quantum field theories. In Section 3, we shall discuss collectivity in these two theories. The Z-graph in nuclear structure and the corresponding connected sea partons will be compared in Section 4. The core polarization will be contrasted with disconnected sea contribution in Section 5. Finally, we will present the latest lattice calculation to reveal the quark and glue components of the proton spin in Section 6.

### 3. Collectivity

Giant resonances in nuclei with large electric and magnetic transition rates can be qualitatively understood as a collective excitation of many particle-hole states in Gerry's schematic model [4]. They have been successfully described in the random phase approximation (RPA) on Hartree-Fock ground states [5]. The RPA diagrams are illustrated in Fig. 3.

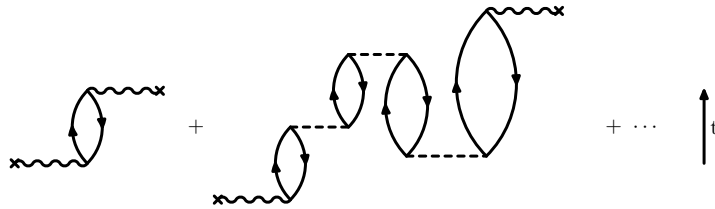


Figure 3: An illustration of the RPA diagrams.

In QCD, the fact that the experimental mass of  $\eta'$  is much larger than all the other Nambu-Goldstone bosons is known as the  $U(1)$  problem and is believed to be related to the  $U(1)$  anomaly of the divergence of the flavor-singlet axial current. The resolution in the context of large  $N_c$  has been given by Witten [6] and Veneziano [7]. In fact, the Veneziano's diagrammatic formulation as illustrated in Fig. 4 is the same as Gerry's schematic model for the degenerate particle-hole states. In the  $U(1)$  case, the collective upward lift from the  $u\bar{u}$ ,  $d\bar{d}$  and  $s\bar{s}$  'would-be' Nambu-Goldstone bosons is due to the constant coupling related to the topological susceptibility of the pure gauge theory.

We see that even though the physics contents of the giant resonance and the  $U(1)$  problem are different, both are the results of collectivity as is the case of BCS superconductivity. Therefore, it is natural to employ similar formulations to tackle them.

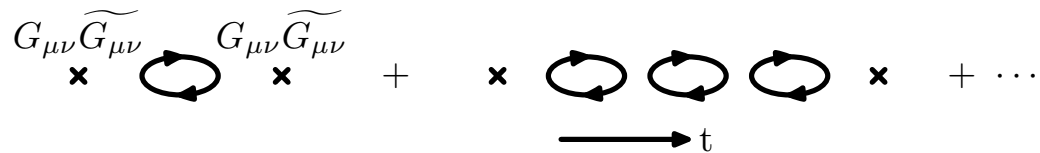


Figure 4: Resolution of the  $U(1)$  problem in Veneziano's diagrammatic approach.

#### 4. Z-graphs and Connected Sea Partons

In many-body theory with time-ordered Bethe-Goldstone diagrams, one inevitably encounters Z-graphs as demonstrated in Fig. 5. This refers to the part of the diagram where the a hole line is still connected to the valence

particle lines when the interaction lines are cut. This is in contrast to the particle-hole bubble in the left diagram where the hole line is disconnected from the valence particle lines when the interaction lines are cut.

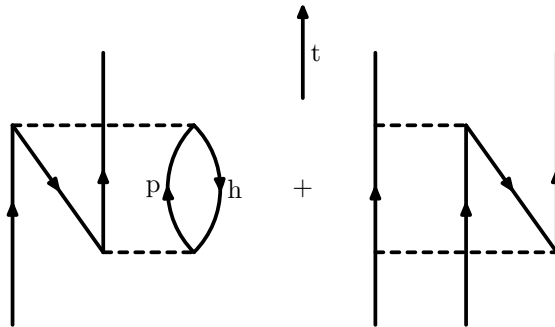


Figure 5: Z-graphs of the Bethe-Goldstone diagrams.

This distinction of the ‘connected hole’ and ‘disconnected hole’ diagrams had not been introduced in the classification of the parton degrees of freedom until the surprisingly large Gottfried sum rule violation was discovered in the deep inelastic scattering (DIS) experiment by the NMC Collaboration [8]. The Gottfried sum rule [9],  $I_G \equiv \int_0^1 dx [F_2^p(x) - F_2^n(x)]/x = 1/3$ , was obtained under the assumption of a symmetric  $\bar{u}$  and  $\bar{d}$  sea [9]. The NMC measurement of  $I = 0.235 \pm 0.026$  implies that the assumption of a symmetric  $\bar{u}$  and  $\bar{d}$  sea was invalid and the  $x$ -integrated difference of the  $\bar{u}$  and  $\bar{d}$  sea is  $\int_0^1 [\bar{d}(x) - \bar{u}(x)]dx = 0.148 \pm 0.039$ . This striking result from the NMC was subsequently checked using an independent experimental technique. From measurements of the Drell-Yan cross section ratios of  $(p + d)/(p + p)$ , the NA51 [10] and the Fermilab E866 [11] experiments clearly observed the  $\bar{u}$  and  $\bar{d}$  difference in the proton sea over the kinematic range of  $0.015 < x < 0.35$ .

In order to understand the origin of this large difference between  $\bar{u}$  and  $\bar{d}$ , an Euclidean path-integral description of the hadronic tensor  $W_{\mu\nu}$  for deep inelastic scattering was formulated [12]. In the Bjorken limit, there are three gauge invariant and topologically distinct diagrams, as shown in Fig. 1. The various lines in Fig. 1 represent the quark propagators from the source of the nucleon interpolation field at time  $t = 0$  to the sink time at  $t$  and the currents are inserted at  $t_1$  and  $t_2$ .

We first note that Fig. 6b, where the quarks propagate backward in time between  $t_1$  and  $t_2$ , corresponds to contributions from the anti-partons which we refer as ‘connected-sea’ (CS)  $\bar{u}^{cs}$  and  $\bar{d}^{cs}$ . In contrast, the time-

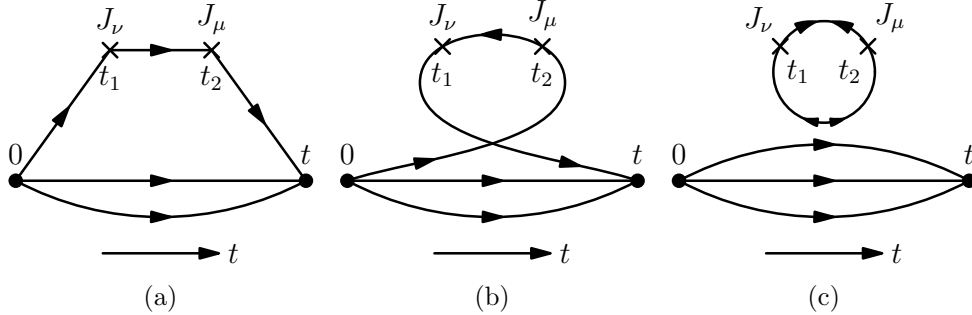


Figure 6: Three gauge invariant and topologically distinct diagrams in the Euclidean path-integral formulation of the nucleon hadronic tensor in the large momentum frame. In between the currents at  $t_1$  and  $t_2$ , the parton degrees of freedom are (a) the valence and CS partons  $q^{v+cs}$ , (b) the CS anti-partons  $\bar{q}^{cs}$ , and (c) the DS partons  $q^{ds}$  and anti-partons  $\bar{q}^{ds}$  with  $q = u, d, s$ , and  $c$ . Only  $u$  and  $d$  are present in (a) and (b).

forward propagating quarks in Fig. 6a correspond to valence and CS partons  $u^{v+cs}$  and  $d^{v+cs}$ , where the valence is defined as  $q^v \equiv q^{v+cs} - \bar{q}^{cs}$  and  $q^{cs}(x) \equiv \bar{q}^{cs}(x)$ . Finally, Fig. 6c gives the disconnected sea (DS)  $q^{ds}$  and  $\bar{q}^{ds}$  for  $q = u, d, s, c$ , since it contains both forward and backward propagating quarks. The nomenclature of connected and disconnected seas follows from those in the time-ordered perturbation theory – CS is the higher Fock-state component in the Z-graphs where the quark lines associated with the current insertions are connected to the valence quark lines; whereas, the DS corresponds to vacuum polarization.

We should point out a fine difference between the CS from Fig. 6b and the connected hole in the Z-graphs as illustrated in Fig. 5. In the path-integral diagram in Fig. 6b, the anti-quarks between the currents at  $t_1$  and  $t_2$  are pre-existing, i.e. they are in the nucleon wavefunction and exist before  $t_1$  and after  $t_2$  just as the case in Fig. 6c so that DIS is measuring the parton density. They are not pair-produced by the hard photon from the lepton-nucleon scattering. The existence of the CS is easily revealed in the path-integral approach owing to the fact that it is a time-ordered formulation as are the Bethe-Goldstone diagrams. In this sense, Fig. 6b can be considered a generalized Z-graph. Similarly, Fig. 6c can be considered a ‘direct diagram’ in the Bethe-Goldstone sense; while Fig. 6b, by the same token, can be considered the ‘exchange diagram’ to reflect the fact that quarks are fermions.

In the isospin limit where  $\bar{u}^{ds}(x) = \bar{d}^{ds}(x)$ , it is proved [13] that the DS do not contribute to the Gottfried sum rule violation. The isospin symmetry

breaking is small and cannot explain the large observed violation. Rather, the majority of the violation could only come from the CS. We see from Figs. 6a and 6b that the CS and the valence are tangled together in one flavor trace. Hence, there is no isospin symmetry between  $\bar{u}^{cs}$  and  $\bar{d}^{cs}$  since the state of the proton, being made up of two valence  $u$  and one valence  $d$ , is not an isospin singlet state. Furthermore, we see that while  $u$  and  $d$  have both CS and DS, strange and charm have only the DS. As far as the small- $x$  behavior is concerned, there is only reggeon exchange for the flavor non-singlet valence and CS, so the small- $x$  behavior for the valence and CS partons is  $q^{v+cs}(x), \bar{q}^{cs}(x) \xrightarrow{x \rightarrow 0} \propto x^{-1/2}$ . On the other hand, there is flavor-singlet pomeron exchange in addition to the reggeon exchange for the DS partons, thus their small  $x$  behaviors are  $q^{ds}(x), \bar{q}^{ds}(x) \xrightarrow{x \rightarrow 0} \propto x^{-1}$ . Since the CS is in the same connected insertions as the valence, it evolves like the valence; whereas, the DS evolves differently in that it has an additional pair-creation kernel from the gluon [12].

While the difference of  $\bar{u}^{cs}(x)$  and  $\bar{d}^{cs}(x)$  can be obtained from  $F_2^p(x) - F_2^n(x)$ , there is not yet a well-established way to directly obtain  $\bar{u}^{cs}(x) + \bar{d}^{cs}(x)$  and, for that matter, separately  $\bar{u}^{cs}(x)$  and  $\bar{d}^{cs}(x)$  from experiments. We have shown a way to achieve this separation with a combination of experiments, the global fit of PDF, and a lattice calculation of the momentum fraction  $\langle x \rangle$  in the DI in Fig. 10b. The recent HERMES semi-inclusive DIS experiment of kaon production on deuteron [14] has produced the strangeness parton distribution function  $s(x) + \bar{s}(x)$  at  $Q^2 = 2.3\text{GeV}^2$ . We have used this data, combined with the ratio of the lattice calculation of the strange and  $u/d$  momentum fractions in the disconnected insertion, and  $\bar{u}(x) + \bar{d}(x)$  from the globally fitted parton distribution function (PDF), to extract  $\bar{u}^{cs}(x) + \bar{d}^{cs}(x)$  in the following formula

$$\bar{u}^{cs}(x) + \bar{d}^{cs}(x) = \bar{u}(x) + \bar{d}(x) - \frac{1}{R}(s(x) + \bar{s}(x)). \quad (1)$$

at  $Q^2 = 2.3\text{GeV}^2$ , where  $\bar{u}(x) + \bar{d}(x)$  is from the CT10 PDF [15] which contains both the CS and DS. The strange parton distribution  $s(x) + \bar{s}(x)$  is from the HERMES data and  $R$  is the ratio of the strange momentum fraction to that of the  $u/d$  in the disconnected insertion in a lattice calculation with dynamical fermions [16]

$$R = \frac{\langle x \rangle_{s+\bar{s}}}{\langle x \rangle_{u+\bar{u}}(DI)} = 0.857(40), \quad (2)$$



In extracting the CS in Eq. (1), we have assumed that the strange parton distribution is proportion to that of  $\bar{u}^{ds}(x)$  so that the proportional constant is  $R$ . In this way, the CS  $\bar{u}^{cs}(x) + \bar{d}^{cs}(x)$  is obtained in Eq. (1) by subtracting the DS from the total  $\bar{u}(x) + \bar{d}(x)$  from CT10 PDF.

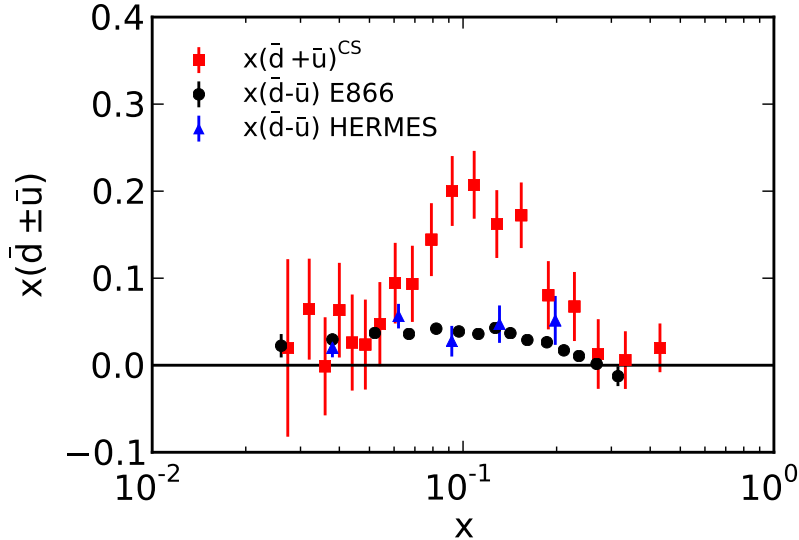


Figure 7:  $x(\bar{d}^{cs}(x) + \bar{u}^{cs}(x))$  obtained from Eq. (1) is plotted together with  $x(\bar{d}(x) - \bar{u}(x))$  from E866 Drell-Yan experiment [17] and from SIDIS HERMES experiment [18].

We plot the distribution function evaluated with Eq. (1), multiplied by the momentum fraction, i.e.  $x(\bar{u}(x) + \bar{d}(x) - \frac{1}{R}(s(x) + \bar{s}(x)))$  in Fig. 7 together with  $x(\bar{d}(x) - \bar{u}(x))$  from E866 Drell-Yan measurement [17] at  $Q^2 = 54 \text{ GeV}^2$  and from semi-inclusive DIS HERMES measurement [18] at  $\langle Q^2 \rangle = 2.3 \text{ GeV}^2$ . We see that  $x(\bar{u}^{cs}(x) + \bar{d}^{cs}(x))$  from Eq. (1) is peaked at medium  $x \sim 0.1$ , the same way as  $x(\bar{d}(x) - \bar{u}(x))$  from E866 and HERMES. This is consistent with the expectation that the small- $x$  of CS, like the valence, behaves as  $x^{-1/2}$  as we alluded to earlier; so that, when CS is multiplied with  $x$ , it would be peaked at medium  $x$ , in contrast to that of the DS, e.g.  $x(s(x) + \bar{s}(x))$  from the HERMES experiment. Furthermore, we note that  $x(\bar{u}^{cs}(x) + \bar{d}^{cs}(x))$  is generally larger than  $x(\bar{d}(x) - \bar{u}(x))$  in this  $x$ -range as it should and is larger by a factor  $\sim 4$  at the peak.

We also plot  $x(\bar{u}(x) + \bar{d}(x) - \frac{1}{R}(s(x) + \bar{s}(x)))$ ,  $x(\bar{u}^{ds}(x) + \bar{d}^{ds}(x)) = \frac{1}{R}x(s(x) + \bar{s}(x))$  and  $x(\bar{u}(x) + \bar{d}(x))$  from CT10 in Fig. 8 to show that the CS and DS

have very different  $x$ -dependence. The different shapes of CS and DS are in good agreement with the expectation discussed earlier. This agreement lends support to the approach we have adopted. It is interesting to note that should a very different value of  $R$  be used, the  $x$ -dependence of CS and DS would no longer agree with expectation.

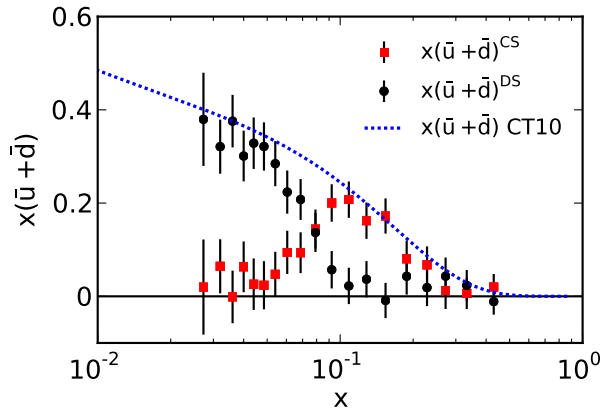


Figure 8:  $x(\bar{u}^{cs}(x) + \bar{d}^{cs}(x))$  obtained from Eq. (1) is plotted together with  $x(\bar{u}(x) + \bar{d}(x))$  from CT10 and  $\frac{1}{R}x(s(x) + \bar{s}(x))$  which is taken to be  $x(\bar{u}^{ds}(x) + \bar{d}^{ds}(x))$ .

Besides having different small  $x$  behavior, the CS and DS evolve differently in the evolution equation [12]. The CS evolves the same way as the valence, while the the DS evolution has an additional contribution from the gluon splitting. The global analyses of PDFs' have not yet incorporated the separate evolutions for CS and DS.

## 5. Core Polarization and Vacuum Polarization

In improving the magnetic moment calculation of one particle outside the closed shell, the core-polarization has been considered which involves the particle-hole excitation as depicted in Fig. 9. This is referred to as the Arima-Horie effect [19] in the nuclear physics literature, as shown in Fig. 9.

In the case of lattice QCD, the nucleon form facts are calculated through the 3-point functions in Fig. 10. The connected insertion in Fig. 10a contains the valence and the CS, while Fig. 10b contains the DS. It is the latter that corresponds to the core polarization in the nuclear structure. For deep inelastic scattering, the valence and CS contributions from Fig. 6a and Fig. 6b

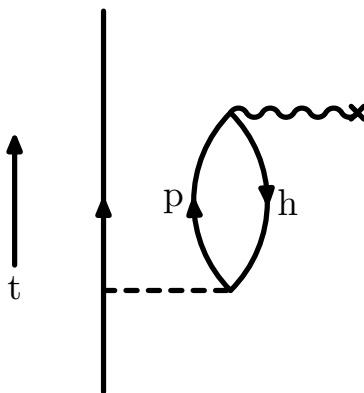


Figure 9: Core polarization diagram of the valance nucleon.

have merged into the moment calculation of Fig. 10a under the operator product expansion (it is the short-distance Taylor expansion in Euclidean path-integral formulation). On the other hand, the DS parton and anti-parton contributions in Fig. 6c has become the sum of DI moments in Fig. 10b.

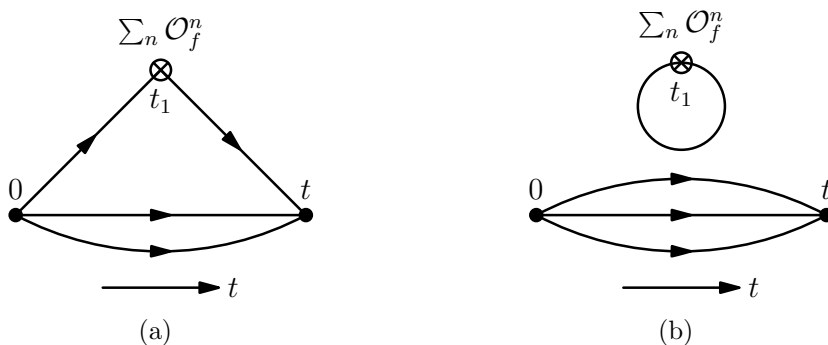


Figure 10: 3-point functions for (a) connected insertions (CI) and (b) disconnected insertions (DI).

## 6. Where Does the Spin of the Proton Come from?

We have done a complete calculation of the quark and glue momenta and angular momenta in the proton [20]. These include the quark contributions from both the connected and disconnected insertions. The quark disconnected insertion loops are computed with  $Z_4$  noise, and the signal-to-noise

is improved with unbiased subtractions. The glue operator is comprised of gauge-field tensors constructed from the overlap operator. The calculation is carried out on a  $16^3 \times 24$  quenched lattice at  $\beta = 6.0$  for Wilson fermions with  $\kappa = 0.154, 0.155$ , and  $0.1555$  which correspond to pion masses at 650, 538, and 478 MeV, respectively. The chirally extrapolated  $u$  and  $d$  quark momentum/angular momentum fraction is found to be  $0.64(5)/0.70(5)$ , the strange momentum/angular momentum fraction is  $0.023(6)/0.022(7)$ , and that of the glue is  $0.33(6)/0.28(8)$ . The previous study of quark spin on the same lattice revealed that it carries a fraction of  $0.25(12)$  of proton spin. The orbital angular momenta of the quarks are then obtained from subtracting the spin from their corresponding angular momentum components. We find that the quark orbital angular momentum constitutes  $0.47(13)$  of the proton spin with almost all of it coming from the disconnected insertions.

In Table 1, we list the quark momentum fractions  $\langle x \rangle \equiv T_1(0)$  for the connected insertion (CI) ( $u$  and  $d$ ) and disconnected insertion (DI) ( $u/d$  and  $s$ ) as well as that of the glue. We also list the corresponding  $T_2(0)$  and total angular momenta fraction  $2J = T_1(0) + T_2(0)$  for each quark flavor and glue. These values are obtained at  $\mu = 2$  GeV in  $\overline{MS}$  scheme after perturbative renormalization and mixing between the quark and glue operators [21].

|                     | CI(u)      | CI(d)      | CI(u+d)   | DI(u/d)   | DI(s)     | Glue       |
|---------------------|------------|------------|-----------|-----------|-----------|------------|
| $\langle x \rangle$ | 0.416(40)  | 0.151(20)  | 0.569(45) | 0.037(7)  | 0.023(6)  | 0.334(56)  |
| $T_2(0)$            | 0.287(112) | -0.221(80) | 0.061(22) | -0.002(2) | -0.001(3) | -0.056(52) |
| $2J$                | 0.703(118) | -0.070(82) | 0.630(51) | 0.035(7)  | 0.022(7)  | 0.278(76)  |
| $g_A$               | 0.91(11)   | -0.30(12)  | 0.62(9)   | -0.12(1)  | -0.12(1)  | –          |
| $2L$                | -0.21(16)  | 0.23(15)   | 0.01(10)  | 0.16(1)   | 0.14(1)   | –          |

Table 1: Renormalized values in  $\overline{MS}$  scheme at  $\mu = 2$  GeV.

We illustrate the composition of proton spin in a pie chart in Fig. 11. The total quark spin constitutes  $25(12)\%$  and the glue also gives  $28(8)\%$ . The rest ( $47(13)\%$ ) comes from the quark orbital angular momentum. Since the  $u$  and  $d$  quark orbital angular momenta in the connected insertion (i.e. valence) almost cancel, almost all of the quark orbital angular momentum comes from the disconnected insertion (i.e. vacuum polarization). We have used the momentum and angular momentum sum rules to obtain the renormalization

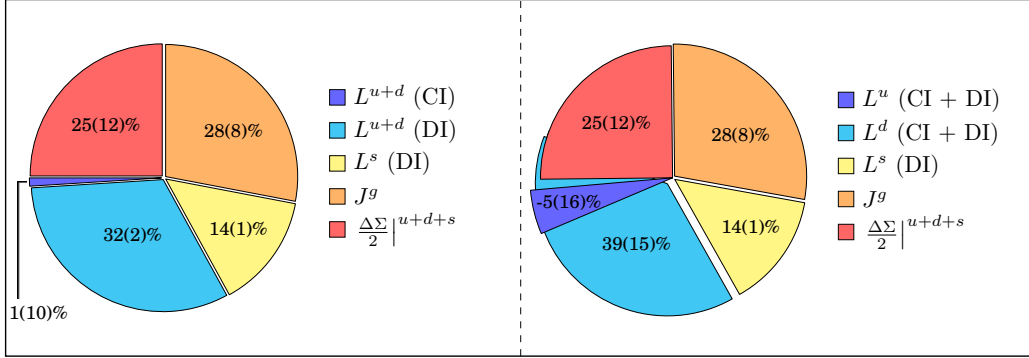


Figure 11: Decomposition of the proton spin in terms of quark spin, glue spin, and quark orbital angular momentum for the  $u, d$  and  $s$  quarks.

constants for the lattice quark and glue energy-momentum tensor operators and used perturbative renormalization and mixing between the quark and glue operators to quote our final numbers in the  $\overline{MS}$  scheme at  $\mu = 2$  GeV. This is the first time that a complete calculation on the decomposition of the proton momentum and spin is carried out.

### 6.1. Quark spin from anomalous Ward identity

Now that we have gone through the complete calculation in the quenched approximation, the next step is to carry out the same calculations with valence overlap fermion on  $2 + 1$ -flavor dynamical domain-wall fermion gauge configurations on several lattices with different lattice spacings and sea quark masses so that we can obtain definitive results of the proton spin components at the physical pion mass and the continuum limit with realistic dynamical quarks in the vacuum in order to compare with experiments and make predictions.

One of the quantities to calculate is the quark spin and the most challenging part is the disconnected insertion. We first calculated the quark loop for the axial-vector current and found that, contrary to the pseudoscalar and scalar cases, it is not dominated by the low modes. As a result, one needs a large number of noises to control the statistical error of the high modes. Instead of increasing the number of noises, we take another approach. We shall calculate the axial-vector matrix element from the anomalous Ward identity

$$\partial^\mu A_\mu^0 = 2 \sum_{f=1}^{N_f} m_f \bar{q}_f \gamma_5 q_f + N_f 2q, \quad (3)$$

where  $q$  is the local topological charge operator. For the overlap fermion, the topological charge is given by the overlap Dirac operator, i.e.  $q(x) = Tr\gamma_5(1 - \frac{1}{2}D_{ov}(x, x))$ . We see from the r.h.s of Eq. (3) that the renormalization of the pseudoscalar density is canceled by the renormalization of the quark mass for overlap fermion and there is no renormalization for the topological term due the index theorem as obeyed by the  $q$  defined by the overlap operator. Therefore, calculating the r.h.s. of Eq. (3) gives the non-perturbatively renormalized axial-vector matrix element which is the quark spin. We show our preliminary results on the topological charge contribution whose signal is coded in the slope of the figure.

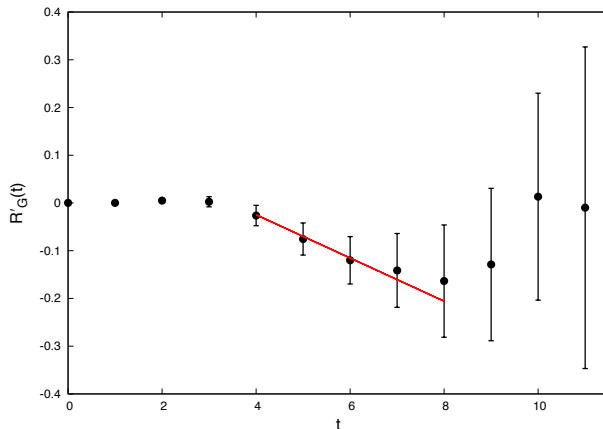


Figure 12: The three-point to two-point function ratio in the sum method as a function of time where the anomaly contribution is the slope of the ratio after the nucleon appears in the two-point correlator. This is at  $q^2 = -0.186 \text{ GeV}^2$ .

The slope is  $-0.045(16)$ . This is done on the  $24^3 \times 64$  lattice with 100 configurations and both the valence and sea quarks are at pion mass of 330 MeV. This is the contribution of the anomaly to the quark spin for each flavor and at  $q^2 = -0.186 \text{ GeV}^2$ . When the  $q^2$  extrapolation to  $q^2 = 0$  and chiral extrapolation to the physical pion are carried out, we expect the number to be larger. The pseudoscalar density contribution turns out to be very small. We are analyzing them with more configurations and with more nucleon sources. A statistical error of 15% is targeted. Production is ongoing for the two  $32^3 \times 64$  lattices with lattice spacings of 0.085 and 0.14 fm. When the continuum and physical pion mass limits are taken, we should have a better picture on the quark spin in the proton.

## 7. Summary

We see that nuclear structure in many-body theory and lattice QCD calculation of nucleon structure share many conceptual similarities in the classification of fermion degrees of freedom and collective phenomena. However, there is a significant difference in that the nucleon structure involves explicit glue contributions which are absent in the study of nuclear structure. Furthermore, there are triangle anomaly and trace anomaly in QCD which have significant consequences in quark spin and nucleon mass. These are novel and challenging features in the study of nucleon structure both theoretically and experimentally.

## Acknowledgments

I thank my colleagues in the  $\chi$ QCD Collaboration for the lattice results. The research is supported partially by the U.S. Department of Energy grant DE-FG05-84ER40154 and the Center for Computational Sciences of University of Kentucky.

## References

- [1] A. Bohr and B.R. Mottelson, *Nuclear Structure*, Vol. II, pp. 416 (W.A. Benjamin, Inc. 1975).
- [2] G.E. Brown, J.H. Gunn, P. Gould, Nucl. Phys., **46**, 598 (1963).
- [3] T.T.S. Kuo and G.E. Brown, Nucl. Phys. **85**, 40 (1966).
- [4] G.E. Brown, Chap. V. 3 in *Unified Theory of Nuclear Models and Forces* (North-Holland Pub. Co. Amsterdam 1971).
- [5] K.F. Liu and G.E. Brown, Nucl. Phys. **A265**, 385 (1976).
- [6] E. Witten, Nucl. Phys. **B156**, 269 (1979).
- [7] G. Veneziano, Nucl. Phys. **B159**, 213 (1979); Phys. Lett. **95 B**, 90 (1980).
- [8] A. Amandruz *et al.* (NMC Collaboration), Phys. Rev. Lett. **66**, 2712 (1991); M. Arneodo *et al.*, Phys. Rev. D **50**, R1 (1994).

- [9] K. Gottfried, Phys. Rev. Lett. **18** 1174 (1967).
- [10] A. Baldit *et al.* (NA51 Collaboration), Phys. Lett. B **332**, 244 (1994).
- [11] E. A. Hawker *et al.* (E866/NuSea Collaboration), Phys. Rev. Lett. **80**, 3715 (1998); J. C. Peng *et al.*, Phys. Rev. D **58**, 092004 (1998); R.S. Towell *et al.*, Phys. Rev. D **64**, 052002 (2001).
- [12] K.F. Liu, Phys. Rev. **D62**, 074501 (2000).
- [13] K.F. Liu and S.J. Dong, Phys. Rev. Lett. **72**, 1790 (1994).
- [14] A. Airapetian *et al.* (HERMES), Phys. Lett. **B666**, 446 (2008).
- [15] H.L. Lai, M. Guzzi, J. Huston, Z. Li, P.M. Nadolsky, J. Pumplin, C.-P. Yuan, Phys. Rev. **D82**, 074024 (2010), [arXiv:1007.2241].
- [16] T. Doi *et al.* ( $\chi$  QCD Collaboration), PoS **LATTICE2008**, 163 (2008), [arXiv:0810.2482].
- [17] R.S. Towell *et al.* (FNAL E866/NuSea Collaboration), Phys. Rev. **D64**, 052002 (2001).
- [18] A. Ackerstaff *et al.* (HERMES), Phys. Rev. Lett. **81**, 5519 (1998).
- [19] A. Arima and H. Horie, Prog. Theor. Phys. **12**, 623 (1954).
- [20] M. Deka, T. Doi, Y.B. Yang, B. Chakraborty, S.J. Dong, T. Draper, M. Glatzmaier and M. Gong, H.W. Lin, K.F. Liu, D. Mankame, N. Mathur, and T. Streue, arXiv:1312.4816 [hep-lat].
- [21] Michael Glatzmaier and K.F. Liu, arXiv:1403.7211.